HYDROLOGICAL PROCESSES
Hydrol. Process. (2011)
Published online in Wiley Online Library
(wileyonlinelibrary.com) DOI: 10.1002/hyp.8418

Passive microwave remote sensing of the historic February 2010 snowstorms in the Middle Atlantic region of the USA

James L. Foster,[1]* Gail Skofronick-Jackson,[1] Huan Meng,[2] James R. Wang,[2,5] George Riggs,[5] Paul J. Kocin,[2] Benjamin T. Johnson,[1,3] Judah Cohen,[6] Dorothy K. Hall[1] and Son V. Nghiem[4]

[1] *Goddard Space Flight Center, NASA, Greenbelt, MD, USA*
[2] *National Environmental Satellite, Data, and Information Service, NOAA, Washington, DC, USA*
[3] *Joint Center for Earth Systems Technology, University of Maryland, Baltimore, MD, USA*
[4] *Jet Propulsion Laboratory, California Institute of Technology, Pasadena, CA, USA*
[5] *Science Systems and Applications, Inc., Lanham, MD, USA*
[6] *Atmospheric and Environmental Research, Inc., Lexington, MA, USA*

Abstract:

The snowfall in the Baltimore/Washington metropolitan area during the winter of 2009/2010 was unprecedented and caused serious snow-related disruptions. In February 2010, snowfall totals approached 2 m, and because maximum temperatures were consistently below normal, snow remained on the ground the entire month. One of the biggest contributing factors to the unusually severe winter weather in 2009/2010, throughout much of the middle latitudes, was the Arctic Oscillation. Unusually high pressure at high latitudes and low pressure at middle latitudes forced a persistent exchange of mass from north to south. In this investigation, a concerted effort was made to link remotely sensed falling snow observations to remotely sensed snow cover and snowpack observations in the Baltimore/Washington area. Specifically, the Advanced Microwave Scanning Radiometer onboard the Aqua satellite was used to assess snow water equivalent, and the Advanced Microwave Sounding Unit-B and Microwave Humidity Sounder were employed to detect falling snow. Advanced Microwave Scanning Radiometer passive microwave signatures in this study are related to both snow on the ground and surface ice layers. In regard to falling snow, signatures indicative of snowfall can be observed in high frequency brightness temperatures of Advanced Microwave Sounding Unit-B and Microwave Humidity Sounder. Indeed, retrievals show an increase in snow water equivalent after the detection of falling snow. Yet, this work also shows that falling snow intensity and/or the presence of liquid water clouds impacts the ability to reliably detect snow water equivalent. Moreover, changes in the condition of the snowpack, especially in the surface features, negatively affect retrieval performance. Copyright © 2011. This article is a U.S. Government work and is in the public domain in the USA.

KEY WORDS snowfall; historical; microwave; AMSR-E; AMSU-B; MHS

Received 10 May 2011; Accepted 10 November 2011

INTRODUCTION AND BACKGROUND

Maryland, Delaware, much of Virginia and southeastern Pennsylvania were in the maximum snowfall zone for the two early February nor'easters (2010) that moved up the Atlantic seaboard of the USA. Both storms were classified as major snowstorms (Category 3 of 5) on the Northeast Snowfall Impact Scale (Figures 1 and 2). These record-setting snowfalls permitted us to assess sensor performance and algorithm maturity of falling snow and snowpack retrievals during extreme snow events. This paper is the first to link Advanced Microwave Sounding Unit-B (AMSU-B) remote sensing observations of falling snow to retrieved snowpack characteristics.

The purpose of this paper is to determine the utility of AMSU-B, Microwave Humidity Sounder (MHS) and Microwave Scanning Radiometer (AMSR-E) sensors in making snowfall and snow water equivalent (SWE) measurements over the relatively challenging Baltimore/Washington and Chesapeake Bay areas, where snowfall often mixes with rain, snow cover is generally patchy and a true multilayered snowpack is rarely established. For this investigation, satellite passive microwave radiometers (AMSR-E, AMSU-B, MHS) that respond to the medium within the field of view (atmosphere, clouds and surface) were used to detect falling snow and to observe snowpack properties. None of these sensors were specifically dedicated or designed to observe only snow. Nevertheless, each one is very near to the optimum frequencies/wavelengths required for observing snowfall and SWE.

According to Gutowski *et al.* (2008), large snowfalls from winter storms are more likely to be attendant with a warming climate, with increases in both snowfall amounts and frequency of occurrence. If this is in fact the case, the historic snowstorms of 2010 in the Middle Atlantic States of the USA as well as in parts of Western Europe, and the 2011 storms in the US southern plains, portions of New England and the UK, may not just be statistical outliers but, instead, events worthy of additional examination and monitoring. East coast snowstorms (east coasts of North America and Eurasia) are perhaps the biggest snow makers anywhere in the world for near sea level locations. Although they do not

*Correspondence to: James L. Foster, Goddard Space Flight Center, NASA, Greenbelt, MD, USA.
E-mail: James.L.Foster@nasa.gov

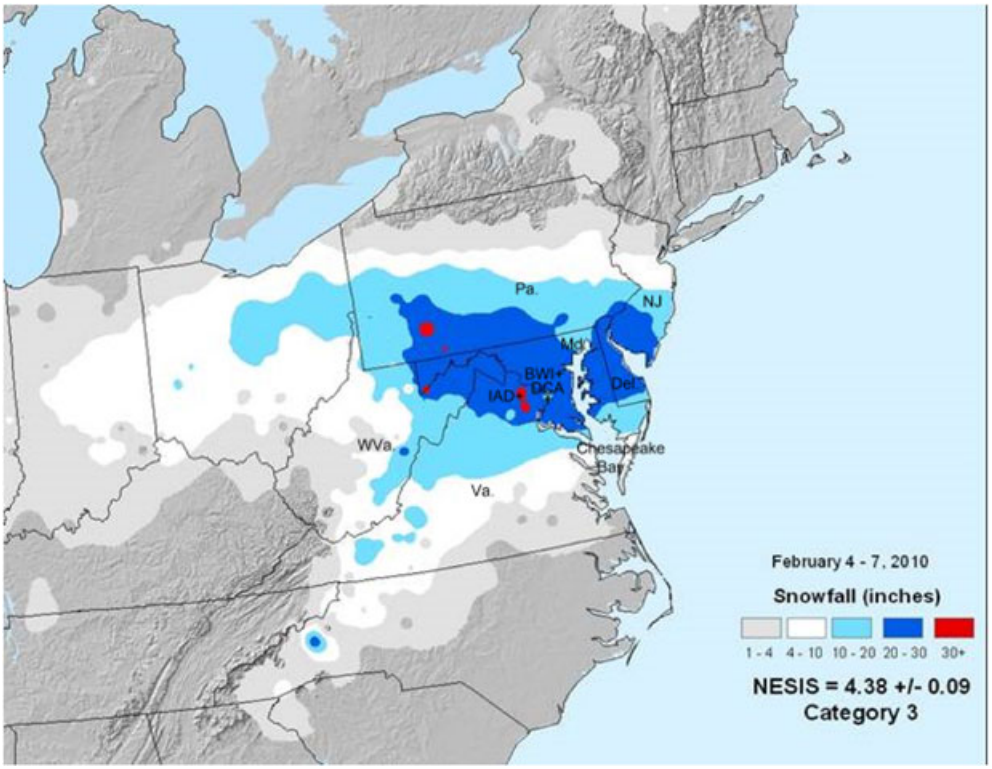

Figure 1. Snow on the ground following the first major snowfall of February 2010 (NOAA, February 2010). Ten inches of snow is equal to approximately 25 cm

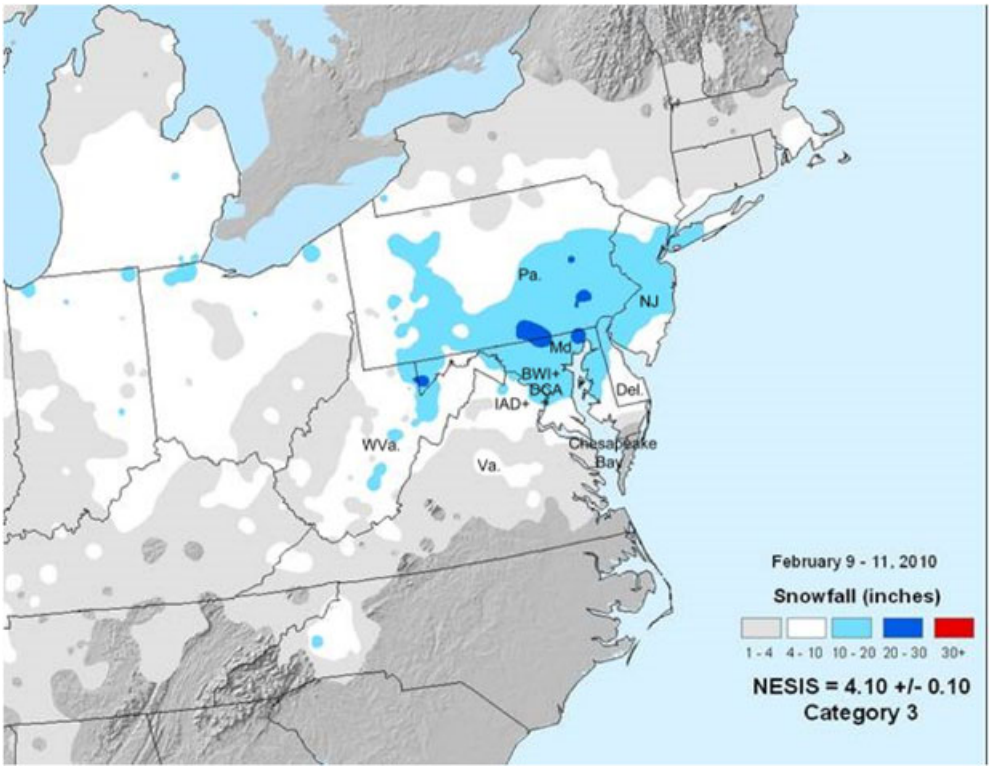

Figure 2. Snow on the ground following the second major snowfall of February 2010 (NOAA, February 2010). Ten inches of snow is equal to approximately 25 cm

typically contribute significantly to the annual water supply of the Middle Atlantic or New England regions, for instance, they can and do bring economies to a standstill.

Because we did not have the luxury of knowing long enough in advance that such historic storms would indeed affect the Middle Atlantic region, we could only study these storms after the fact. Furthermore, because no planned/funded field programmes were in place that would allow us to quantitatively assess the effectiveness of the snowfall and SWE algorithms (simple models

DOI: 10.1002/hyp

designed to derive certain parameters) and to validate their performance during an entire winter season, the results shown here are limited by a lack of available data.

The intent of this work is not to show the relationship between passive microwave-derived snow retrievals and measured SWE or snow depth (SD). It has been long established that such relationships exist. Dozens of regressions have been performed over the past 30 plus years (e.g. Foster *et al.* (1984), Kelly *et al.* (2003), Hallikainen *et al.* (2004) and Chang *et al.* (2005)). However, there is also a growing set of literature describing shortcomings, systematic errors and uncertainties in SWE algorithms that use passive microwave data (e.g. Walker and Goodison (2000), Foster *et al.* (2005), Davenport *et al.* (2010), Clifford (2010) and Tedesco *et al.* (2010)).

Meaningful relationships between passive microwave brightness temperatures (Tb) and falling snow have been proven to exist (e.g. Skofronick-Jackson, *et al.* (2004), Chen and Staelin (2003), Kongoli *et al.* (2003)). Rather, we will show that falling snow signals can be detected with microwave sounders where snow on the ground is retrieved from microwave radiometers. Because both snowfall and SWE algorithms are, in general, insensitive to small amounts of snowfall/snow on the ground, larger snowfalls in data-rich areas provide an opportunity to assess how they will work in more optimal conditions. If they perform poorly under these conditions, it is highly unlikely that they will be useful in more ordinary snow events. However, for SWE retrievals, even in extreme events where signals are strong, liquid clouds as well as surface and snow variability adversely impact the SWE and snowpack retrieval performance. On the other hand, for falling snow detection, dry atmospheric conditions and snow-covered surfaces reduce the effectiveness of the falling snow detection algorithm. But, intense falling snow events, such as the February 2010 storms investigated in this study, can overcome these limiting factors in snow detection retrievals. In such cases, there is the potential for real-time detection of snowfall amounts/intensity over large geographic areas.

This paper begins with a section describing the weather conditions and snowstorm characteristics and then Sections on Sensors and Algorithms, Results, Discussion and Conclusions.

STORM CHARACTERISTICS

On 5–6 February 2010 and then again on 9–10 February 2010, there were two major snowstorms affecting the Washington DC metropolitan area. In both storms, but more notably the first, the polar jet stream was positioned to favour a storm track that moved along the coastal Southeast and Middle Atlantic regions, drawing moisture from both the Gulf of Mexico and the Atlantic Ocean. Atmospheric water vapour was drawn northward not only from the Gulf of Mexico but also from the western Caribbean Sea. Unlike most years, these lows did not track along the coast toward New England but instead idled off the Middle Atlantic region (Cape Charles and Cape Hatteras), which often serves as a focal point for cyclogenesis (Kocin and Uccellini, 2004a), before heading out to sea. It is off these concave-shaped capes that East Coast storms markedly deepen.

The twin storms set all-time records at Marshall/Baltimore–Washington International Airport (BWI), where 63 cm was measured in the first storm on 5–6 February 2010 and at Dulles International Airport (IAD), about 48 km west of Washington, where 81 cm of snow fell, easily surpassing the previous record by 23 cm. Reagan National Airport (DCA) received 45 cm (Figure 1; Kocin and Uccellini, 2004b). In round two on 9–10 February 2010, BWI recorded nearly 50 cm, and both IAD and DCA registered approximately 30 cm (Figure 2). In this second nor'easter, because atmospheric pressures were lower in the storm centre and pressure gradients steeper, strong winds were prevalent and blizzard conditions (wind gusts over 15.6 m/s for 3 h or longer and visibility less than 0.6 km) were encountered for much of the event.

Accumulations at a number of locations in the Baltimore/Washington area exceeded 135 cm during the 6-day period from 5 to 10 February. Less than 5 cm of snowfall was recorded at the aforementioned stations after 10 February. Not surprisingly, these snow events caused significant impacts to transportation; some roads were not ploughed for a week, and some public schools were closed for 10 days. During the 2009/2010 season, DCA's snow total of 149 cm bested the previous snowiest winter mark set in 1898/1899. BWI and IAD easily broke their prior snowfall records, observing 203 cm and 196 cm, respectively.

February weather conditions

February 2010 was the snowiest month ever recorded at nearly every meteorological station in Virginia, Maryland and Delaware and at numerous stations in New Jersey and North Carolina. Although a wet month, it was not exceptionally wet, but nearly all of the precipitation fell as snow. Monthly precipitation (melted snow) at IAD was 11.76 cm or approximately 7.75 cm above the 30-year mean, and at BWI, 10.54 cm was observed or approximately 3 cm above the 30-year mean (NOAA, 2010; Smith, 2010).

There were no remarkable cold air outbreaks; rather, prolonged cold gripped the region. During February, temperatures were consistently below normal nearly every day the entire month. At BWI, the average maximum temperature was 3.2 °C and the average minimum was −4.4 °C, approximately 4.5 and 1.2 °C below normal, respectively. Moreover, the maximum temperature never exceeded 10 °C. At DCA, the average February maximum temperature was 4.1 °C (4.0 °C below normal) and the average minimum was −2.1 °C or 0.9 °C below normal (NOAA, 2010; Smith, 2010).

Persistent cold together with the abundant snowfall permitted snow to remain on the ground throughout the month and into early March, at least on north-facing slopes and in areas away from buildings. For example, at

DOI: 10.1002/hyp

BWI, the average monthly depth was 28 cm; at Dulles, it was 25 cm and at DCA, it was 20 cm. The maximum SD at BWI and IAD was 86 and 66 cm, respectively (NOAA, 2010). These lingering snowpacks allowed us to retrieve SWE from AMSR-E for extended periods.

Atmospheric circulation

The Arctic Oscillation (AO) or Northern Annular Mode is the dominant mode of Northern Hemisphere extratropical climate variability (Thompson and Wallace, 2000). One of the biggest contributing factors to the unusually severe winter weather in 2009/2010, throughout much of the middle latitudes, was the unusually high pressure at high latitudes and low pressure at middle latitudes, forcing a persistent exchange of mass from north to south. This seesaw pressure pattern is a signature of the AO index (Cohen *et al*. (2010) and Seager *et al*. (2010)).

During the winter of 2009–2010, the major teleconnection patterns of the Northern Hemisphere, El Niño/Southern Oscillation and the AO were of moderate to strong amplitude. When El Niños are in place, the southeastern US tends to receive more precipitation in winter than normally would be expected. The observed AO of 2009–2010 was a record negative value going back to at least 1950 (Cohen *et al*., 2010). Often during negative AO winters, Arctic outbreaks (colder air) are more frequent in the eastern US.

Cohen *et al*. (2010) showed that the dominant Northern Hemisphere winter circulation pattern originated with a two-way stratosphere–troposphere interaction that was forced by Eurasian land surface and lower tropospheric atmospheric conditions during autumn. The negative AO was observed throughout the troposphere. This is expected as Baldwin and Dunkerton (1999, 2001) demonstrated that the AO is often of coherent phase throughout the atmospheric column. In fact, the surface AO can be traced back in time to originate in the middle stratosphere. It propagates through the lower stratosphere and then through the entire troposphere on a timescale of 1–2 weeks. This atmospheric configuration, having a fully coupled troposphere and stratosphere and related to a strongly negative AO, forced Arctic air unusually south. Using a skillful winter temperature forecast, it was shown by Cohen *et al*. (2010) that the AO in 2009/2010 explained a greater variance of the observed temperature pattern across the extratropical landmasses of the Northern Hemisphere than did El Niño/Southern Oscillation.

SENSORS AND ALGORITHMS

For detecting falling snow

The atmospheric water vapour AMSU-B sensors on the NOAA-15, NOAA-16 and NOAA-17 satellites, along with the MHS on the NOAA-18 and European meteorological operational satellites, are cross-tracking, scanning, passive microwave sounders (e.g. Ferraro *et al*., 2005). The channel resolution is ~16 km at nadir and ~26 km at the furthest scan angle along track. In fact, the original design purpose of the AMSU-B/MHS sensors was to measure water vapour profiles. However, the 89, 150, 183 ± 1, ± 3, ± 7 GHz channels of AMSU-B can also be used to detect and estimate falling snow (e.g. Skofronick-Jackson *et al*., 2004; Noh *et al*., 2009) as can the AMSU-B follow-on MHS instrument, which employs frequencies of 89, 157, 183 ± 1, ± 3 and 190 GHz. The channels at frequencies near the water vapour line of 183.3 GHz are quite opaque because of atmospheric absorption and are generally referred to as sounding channels, in contrast to the more transparent channels at 89 and 150 GHz as well as the AMSR-E channels that fall in the window region of the atmospheric absorption spectrum.

An AMSU land snowfall detection (LSD) product (Kongoli *et al*., 2003) is generated operationally at the National Environmental Satellite, Data, and Information Service of the National Oceanic and Atmospheric Administration. For more on this, see http://www.osdpd.noaa.gov/ml/mspps/rainprd.html. A set of statistically derived criteria involving all five of AMSU-B/MHS channels and the 23.8 and 53.6 GHz channels on AMSU-A is employed to detect snowfall and filter out false detections triggered by snow on the surface. In general, the LSD algorithm is robust at capturing different types of storm events with a low false detection rate (Kongoli *et al*., 2003). However, false detections are still noticeable when snow is misclassified as rainfall, or snow on the ground mimics snow in the atmosphere.

An improvement was recently made to the LSD algorithm by utilizing the temperature and water vapour profiles from the Global Data Assimilation System dataset (Yan *et al*., 2008). A set of criteria for temperatures at 700 and 850 mb and the surface is set to reclassify precipitation type. For detected snowfall, relative humidity at 700 and 850 mb is used to mitigate false detections. The improved LSD algorithm was tested and reported herein on the 5–6 February snowstorm.

There are several conditions that can affect the falling snow detection performance. The surface conditions and the type and vertical structure (total ice water path in the cloud and cloud depth) of a snow event (e.g. lake effect, synoptic, blizzard) affects the observed Tb values (Skofronick-Jackson and Johnson, 2011). As such, the performance of falling snow retrieval algorithms is dependent on the surface, atmospheric and snow–cloud conditions. Although SWE retrievals rely on channels less than or equal to 89 GHz (e.g. AMSR-E), these lower frequency channels are extremely sensitive to the condition of the snowpack and the ground during falling snow events. During liquid rain events, these channels respond strongly to the absorption and emission from rain drops, which obscure the surface. On the other hand, the higher frequency channels (i.e. AMSU-B/MHS), both sounding and window channels, are sensitive to frozen hydrometeors in clouds.

It should be mentioned that in lighter snowfall events, the contrast is not strong between the signal from falling snow and snow cover on the ground. This makes it difficult to distinguish (detect) falling snow over snow-

DOI: 10.1002/hyp

covered surfaces, especially for the 89 and 150 GHz window channels. In addition, the footprints of AMSU-B/MHS range between ~16 km at nadir and ~26 km at the edge of the cross track scan. There can be considerable variability in the scene's surface and atmospheric features within these larger footprints.

SWE retrievals

The AMSR-E, on board the Earth Observing System Aqua satellite, was launched in 2002. It is the most recent addition to the passive microwave suite of instruments, sensing at the frequencies of 6.9, 10.7, 18.7, 23.8, 36.5 and 89 GHz. AMSR-E snowpack products (Kelly *et al*., 2003, Kelly, 2009) are archived and distributed through the National Snow and Ice Data Center and are available in the Equal Area Scalable Earth Grid projection (at a 25 km × 25 km grid scale). Equal Area Scalable Earth Grid is based on the Lambert Azimuthal Equal Area projection.

In essence, to derive SD, we examine how microwave energy at the various AMSR-E channels is scattered by snow crystals. The greater the depth or density of the snowpack, the more snow crystals are available to scatter the upwelling microwave energy and thus, the lower the Tb. Differences in Tb between channels are used to estimate SD. In the AMSR-E algorithm we employ, if the 18 GHz (vertical polarization) frequency Tb is greater than 252 K and the 36 GHz (vertical polarization) frequency Tb is greater than 245 K, SWE is considered to be zero. The effects of fractional forest cover and forest density on SWE retrievals are also considered by utilizing the University of Maryland Vegetation Continuous Fields data product (Hansen *et al*., 2003). The difference between the 18 and 36 GHz channels to maximize spatial resolution in forested areas and the use of 10V–36V (increased dynamic range) and 10V–18V for deep snow, is scaled through optimization of validation data — optimized empirically based on 2002–2003 in situ data. The inverse of the polarization difference was logged (base 10), and this value was used in the expression.

Melting snowpacks cause the algorithm to report too little snow as the loss tangent increases rapidly, and thus, the scattering albedo is near zero (Foster, 1995). For more about the AMSR-E algorithm, see Kelly (2009).

For estimation of SD, the following general procedure is followed:

$$\mathrm{SD} = ff(\mathrm{SD_f}) + (1 - ff) * (\mathrm{SD_o}) \quad (1)$$

where SD is the total sample snow depth, $\mathrm{SD_f}$ is the SD from the forest component of the instantaneous field of view and $\mathrm{SD_o}$ is the SD from non-forested component of the instantaneous field of view. The quantity *ff* is the forest fraction (where 1.0 = 100% forest fraction and 0.0 = 0% forest fraction).

$$\mathrm{SD_f[cm]} = 1/\log_{10}(\mathrm{pol_{36}}) * (\mathrm{Tb_{18V}} - \mathrm{Tb_{36V}})/(1 - fd\mathrm{x}0.6) \quad (2)$$

$$\mathrm{SD_o[cm]} = [1/\log_{10}(\mathrm{pol_{36}})\mathrm{x}(\mathrm{Tb_{10V}} - \mathrm{Tb_{36V}})] + [1/\log_{10}(\mathrm{pol_{18}})\mathrm{x}(\mathrm{Tb_{10v}} - \mathrm{Tb_{18V}})] \quad (3)$$

where *fd* is the forest high spatial resolution (500 m) density (g cm^{-3}) from the Vegetation Continuous Fields data product (Hansen *et al*., 2003), circularly smoothed at 15-km diameter and re-gridded globally in 1-km grid cells. In Equations [2] and [3], $\mathrm{pol_{36}} = \mathrm{Tb_{36V}} - \mathrm{Tb_{36H}}$ (note that if $\mathrm{pol_{36}} < 1.1$, then $\mathrm{pol_{36}} = 1.1$ to ensure $\log(\mathrm{pol_{36}}) > 0$) and $\mathrm{pol_{18}} = \mathrm{Tb_{18V}} - \mathrm{Tb_{18H}}$ (note that if $\mathrm{pol_{18}} < 1.1$, then $\mathrm{pol_{18}} = 1.1$ to ensure $\log(\mathrm{pol_{18}}) > 0$).

Snow water equivalent is estimated as the product of SD and snow density. To convert SD to SWE, density measurements from data sets of Brown and Braaten (1998) were mapped to the Sturm *et al*. (1995) seasonal snow classification. For more detailed information about passive microwave algorithms, see Foster *et al*. (1997) and Kelly (2009).

Passive microwave snow data products are available globally, every day. The data are projected into 25-km grid cells of the Equal Area Scalable Earth Grid, according to the geographic coordinates of the centre of the field of view of the radiometers. Clouds and darkness generally do not preclude snow detection in the microwave frequencies employed by AMSR-E.

There are several concerns when retrieving SD and SWE from passive microwave algorithms (Clifford, 2010). As mentioned, meltwater in the snowpack can raise the microwave Tb, especially at frequencies above about 30 GHz. SWE is difficult to extract under these conditions; therefore, to minimize the mapping of wet snow, only nighttime data have been used in this study. This alleviates snowmelt effects because refreezing occurs at lower nighttime temperatures (Derksen *et al*., 2000; Foster *et al*., 2005). Additionally, emission from trees can seriously confound the scattering signal of snowpacks (Foster *et al*., 2005). SD and SWE beneath the most densely forested stands that exist in portions of the Middle Atlantic region will not be accurately estimated. Moreover, large bodies of water, such as the Chesapeake Bay and wide-mouthed rivers that empty into it, may affect our ability to estimate SWE if water covers more than approximately 10% of the pixel area.

RESULTS

In this section, we report the results for falling snow and SWE retrievals. For the falling snow retrievals, because the second event had blizzard conditions with significant blowing snow, which would confuse near-surface snow detection, we focused on the results for the 5–6 February 2010 storm. The time series of snowfall rates for this storm at BWI (39.2°N, 76.7°W), IAD (38.95°W, 77.45°) and Charlottesville (CHO) (38°N, 78.5°W) are shown in Figure 3; the locations of these stations are shown in Figure 4(b). For the snowpack retrievals, we chose to present results starting in early February and through early March to investigate the transitioning of the

DOI: 10.1002/hyp

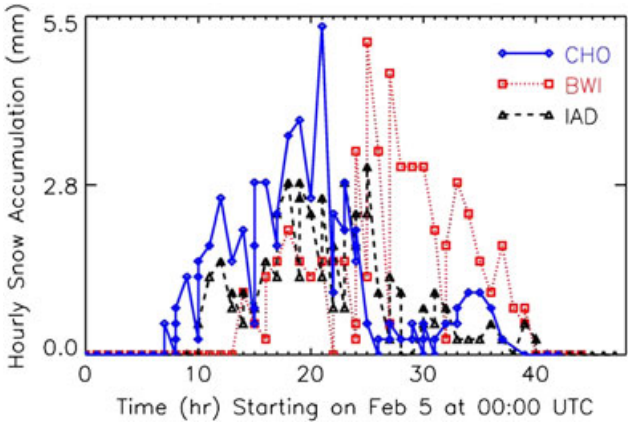

Figure 3. Time series of hourly snow accumulation (water equivalent) at Marshall/Baltimore–Washington International Airport, Dulles International Airport and Charlottesville, VA during the 5–6 February snowstorm. The origin corresponds to 5 February at 00:00 UTC. The local time is UTC minus 5 h

snowpack, SWE and SD, through the two major snow events and subsequent freezing and melting cycles.

Falling snow observations and results

The images in Figure 4 show the 150 GHz Tbs for selected AMSU-B and MHS overpasses on 5–6 February over the Baltimore/Washington area. The 150 GHz channel shows a strong response (cooling) when falling snow is present and produces a decrease in the Tb of 30–60 K (Figure 4(b)–(h)) below the background temperature of ~250 K, which was based on Tbs during clear air overpasses prior to the 5–6 February storm. The 89 and 183 ± 7 GHz channels (not shown) are also responsive to falling snow. In clear air, however, snow-covered and ice-covered land surfaces can have similar Tbs as when falling snow is present. For example, on 4 February (Figure 4(a)), when the ground was relatively snow-free, the Tbs are warmer than 240 K, whereas on 7 February, after the snow has been deposited (Figure 4(i)), the Tbs are colder than 240 K, with the exception of the lowermost portion, which is likely moist soil or a melting snowpack.

High variability exists in the observed 150 GHz conditions because of falling snow and surface emission within the field of view. With overpasses near 0600, 1800, 2100 and 2300 coordinated universal time (UTC), the diurnal temperature conditions also affect the surface temperatures and hence, the surface emission, which is essentially a product of surface temperature and emissivity. Local time is UTC minus 5 h, so the 2100 UTC time is 1600 local time, near the warmest part of the day and may be a prime reason that Figure 4(b)–(d) and (g)–(i) have warmer Tb values in the southern regions of the image. Another part of this variability is because of the cross-track scanning nature of the AMSU-B/MHS instrument that causes mixing of polarizations and slant path angles through the falling snow cloud profiles.

Figure 5 shows the time sequence of the detected snowfall (blue colours) for this storm along with ground observations (closed stars in Figure 5) where falling snow was measured. The majority of the areas where snowfall is occurring (compare the blue coloured detection areas in Figure 5 with the closed stars) were captured by the satellite algorithm from the onset of the storm, around

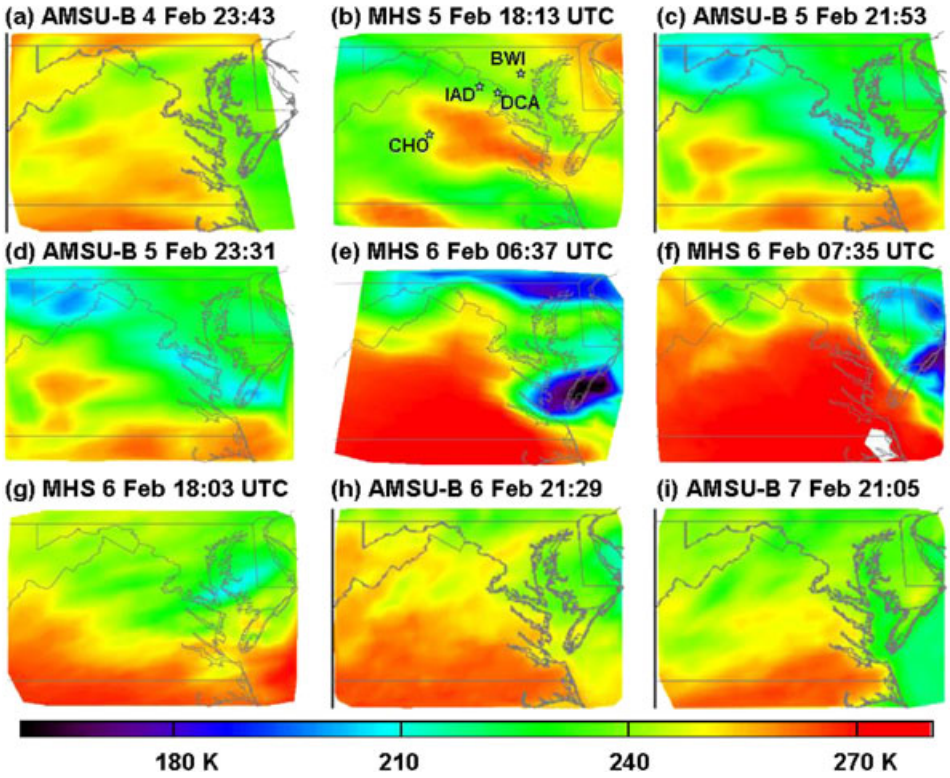

Figure 4. Advanced Microwave Sounding Unit-B and Microwave Humidity Sounder 150 GHz time series for 5–6 February 2010 showing decreases in brightness temperature when falling snow is present. The local time is UTC minus 5 h. The images at (b)–(h) roughly correspond to Figure 3 times of 18, 22, 24, 31, 32, 42 and 46 h, respectively

DOI: 10.1002/hyp

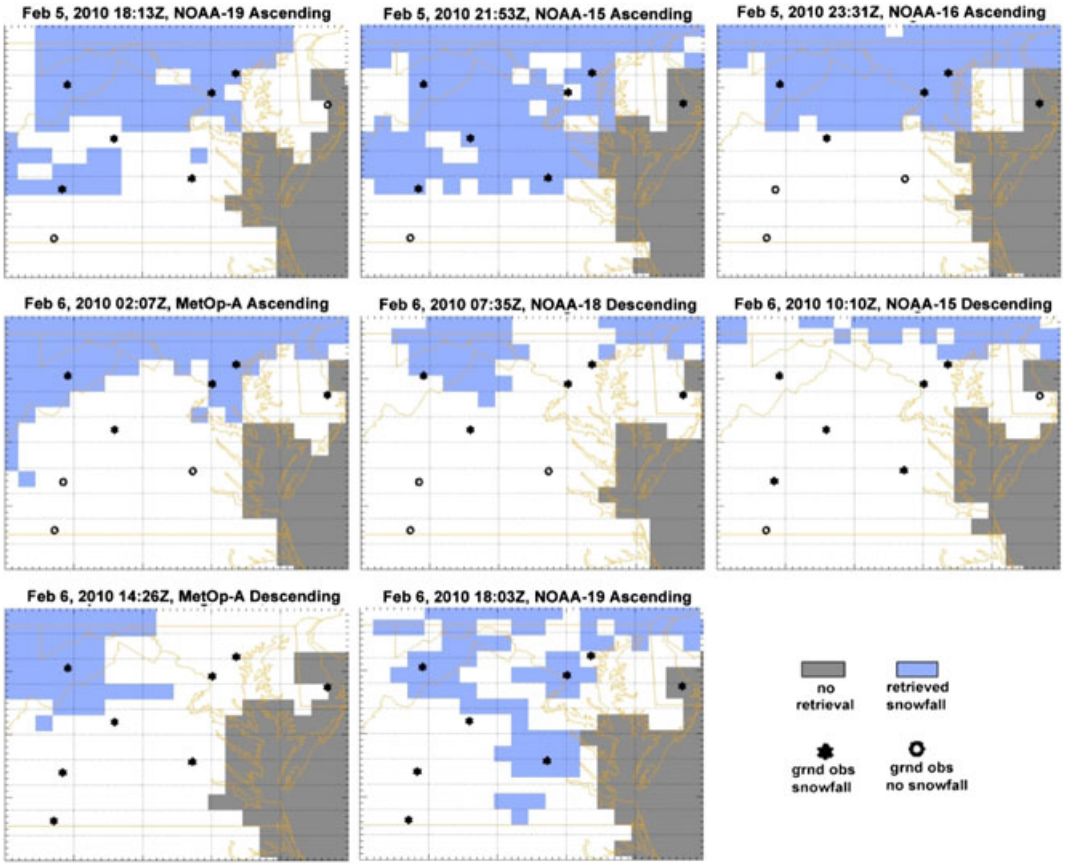

Figure 5. Time sequence of Advanced Microwave Sounding Unit/Microwave Humidity Sounder detected snowfall for the 5–6 February 2010 snowstorms with ground observations

1800 UTC on 5 February to about midnight of the same day. The undetected snowfall areas increased progressively afterwards, with the 1010 UTC pass on 6 February missing most of the snowfall in the study area. The snowfall detection recovered gradually from this point on.

The diminished performance of the LSD algorithm was attributed to the incursion of a dry air mass at least at middle troposphere and above (Figure 6). Because the 183 sounding channels and 150 GHz channel are heavily influenced by water vapour, the Tbs at these channels become warmer in a drier atmosphere, and the signal from snowfall weakens significantly (Figure 4(e) and (f)). Under such a condition, the interrelationships of the channels no longer satisfy the prevailing snowfall conditions for which the LSD algorithm was developed, causing poor detection performance. It is noted that the LSD algorithm worked well throughout this snow event in the Pennsylvania area, where water vapour was consistently high. Similar results are expected for the snow event during 9–10 February, although the blowing and drifting snow encountered during this storm adversely affected ground truth measurements and observations of near surface *versus* atmospheric falling snow. No other snowfall events during the month were intense enough to be detected.

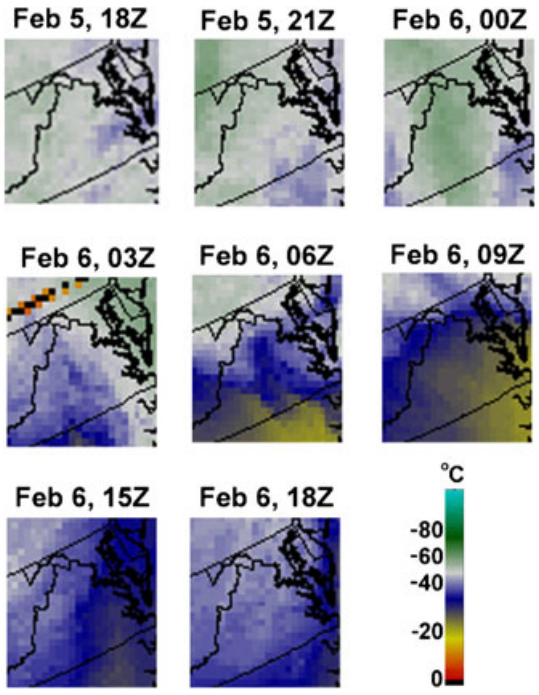

Figure 6. Time sequence of the GOES-11/GOES-12 6.5 μm (water vapour channel) composite images for the 5–6 February 2010 snowstorms. Colder temperatures (green) indicate more moisture in the mid-troposphere and correlate with where the snow detection algorithm performs well. Warmer (blue/yellow) temperatures indicate regions of dry air and correlate with poor algorithm performance. These warmer temperatures also appear in the 150 GHz brightness temperature images in Figure 4e and f

Snowpack observations and results

The image sequences in Figure 7 show SWE values for the period from 1 February 2010 to 3 March 2010. SDs

DOI: 10.1002/hyp

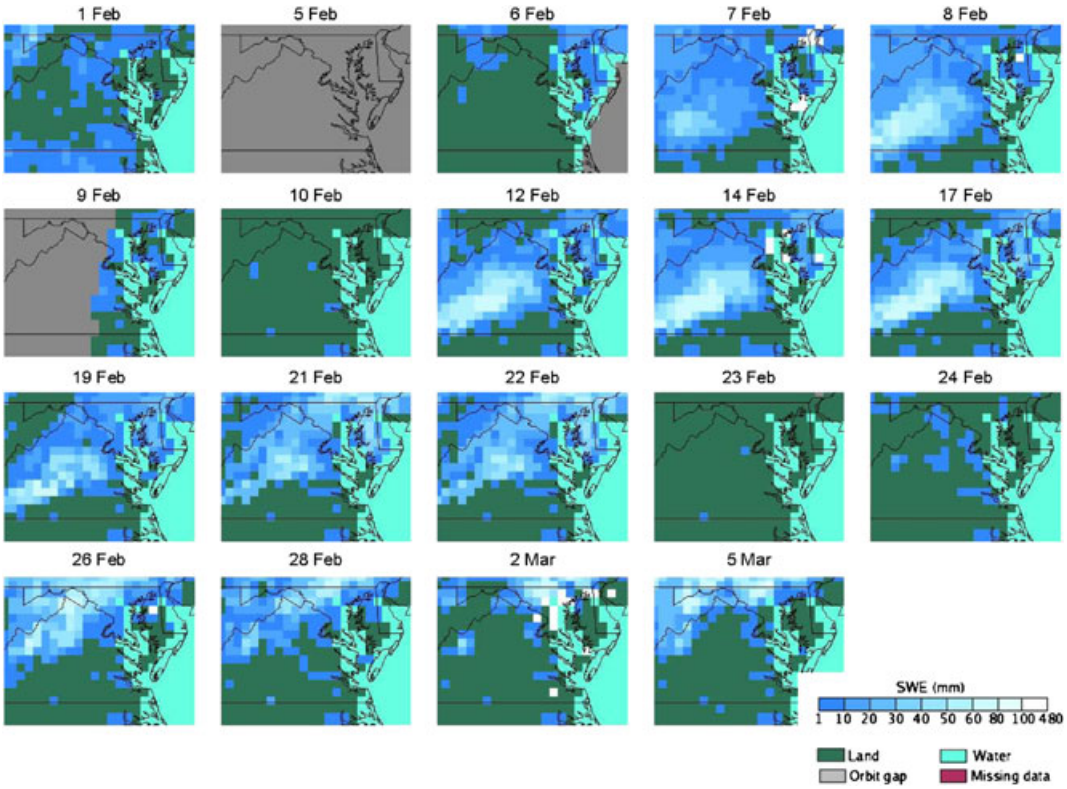

Figure 7. Microwave Scanning Radiometer retrieved snow water equivalent sequence from 1 February 2010 to 5 March 2010

derived from AMSR-E for four ¼ degree × ¼ degree pixels immediately to the west of Washington, DC and from ground-based observations within this area are plotted in Figure 8. In early February, there were some missing data as a result of orbital gaps and/or data not being acquired because of sensor problems. However, on the 7th and 8th, SWE values up to 60 mm (pale blue colour) in central and southwestern Virginia are evident, which correspond to the detection of falling snow on 6 February (Figures 4 and 5). There were no misidentifications of snowfall – when snowfall was retrieved, SWE was also retrieved. When comparing the AMSU-B 150 GHz image on 7 February (Figure 4(i)) with the SWE image on the same day (Figure 7), the areas where SWE exists are cooler in the AMSU-B image. Conversely, on the lower right of this image (tidewater area of the Chesapeake Bay), where SWE retrieved is zero, the Tb values are highest in the AMSU-B images. Additionally, the Moderate Resolution Imaging Spectroradiometer snow cover map on 7 February 2010 (Figure 9) indicates that this area is snow-free.

For the 5 and 6 February storm, AMSR-E retrieved SD values for 25-km grid cells were plotted *versus* interpolated SD values (over the same cells) from airport weather stations, volunteer observers and cooperative observing stations for Maryland and northern Virginia. AMSR-E SWE was converted to SD by using a density value of 250 kg/m^3. Although the maximum AMSR-E estimates of SD were comparable with the maximum interpolated *in situ* measured depths (76 cm), because

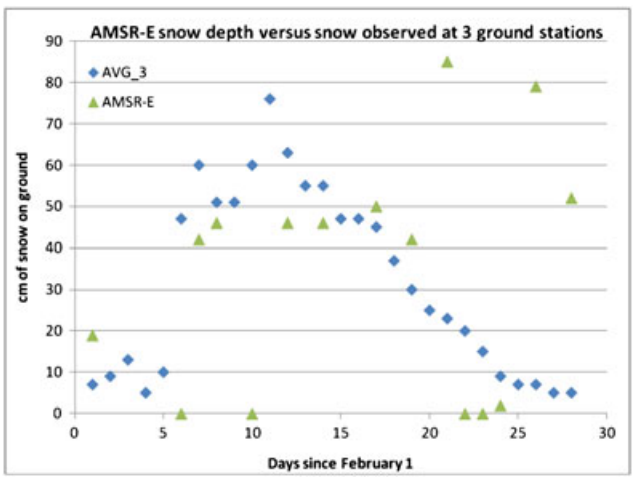

Figure 8. Snow depth derived from Microwave Scanning Radiometer (cm) averaged over four pixels *versus* snow depth averaged for three observation stations

DOI: 10.1002/hyp

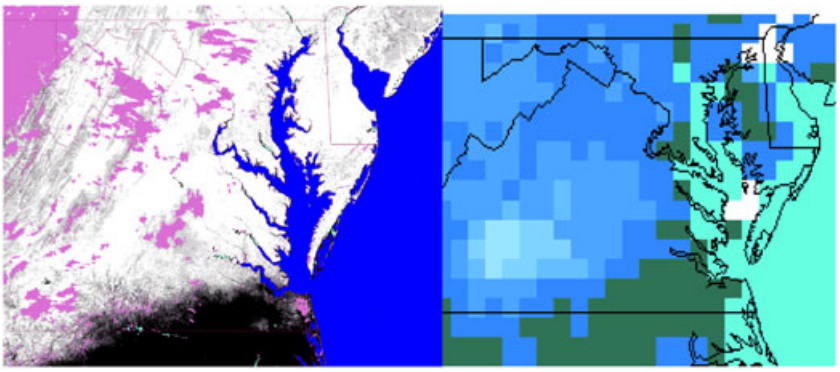

Figure 9. Moderate Resolution Imaging Spectroradiometer fractional snow cover map for 7 February (left) and Microwave Scanning Radiometer snow map also for 7 February. Note position of snowline (areas in black are snow-free). Pink colours on Moderate Resolution Imaging Spectroradiometer image are clouds. As on previous figure, light blue colours represent snow water equivalent values of more than 60 mm and royal blue colours represent snow water equivalent values of less than 10 mm. Green is snow-free land. Turquoise colours are pixels covered mostly or all by water

there was little variation in SD across Maryland and northern Virginia with this storm, the correlation was weak, 0.3. However, when only those pixels having microwave-derived SD of more than 50 cm were used, the correlation was much stronger, 0.675.

On 6 February and again on 10 February (Figure 7) when heavy snow was falling, SWE is derived but the values are negligible, despite the fact that well over 40 cm of snow covered most of the Baltimore/Washington region (Figure 8). For more about this, see the Section on Discussion.

Looking at the images from 12 to 19 February in Figure 7, it can be seen that now, SWE values exceed 100 mm in a few pixels, and in central and southwestern Virginia, the area of greatest SWE (60–100 mm) has expanded. However, in the Baltimore/Washington vicinity, SWEs are much more modest; <30 mm. Both AMSR-E and the Special Sensor Microwave Imager/Sounder, onboard the US Air Force Defense Meteorological Satellite Program series of satellites (Figure 10), portray similar geographic SWE distributions. Although there are numerous observing stations in the densely populated Baltimore/Washington area, there are few available measurements of SWE.

From 21 to 24 February (Figures 7 and 8), the snowpack, although melting, did not completely melt away as evidenced by the image of 26 February, which has a strong SWE signature. This is discussed more in the following section. It is curious that SWE is much more obvious in the metropolitan Baltimore/Washington area on 21, 26 and 28 February 2010, for instance, than earlier in the month. The thickness of the pack did not suddenly increase here nor were air temperatures colder.

For Figure 8, the AMSR-E pixels were selected in a location free of bodies of water, dense forests and large elevation differences. It can be seen from 1 to 19 February that on those days when snow is detected on AMSR-E, the station observations and passive microwave results match up reasonably well – deep snow is recorded from the station data and AMSR-E alike. However, later in the month, the AMSR-E depths are much higher than the station observations. Days when AMSR-E values are not plotted are results of both a sensor anomaly (early in

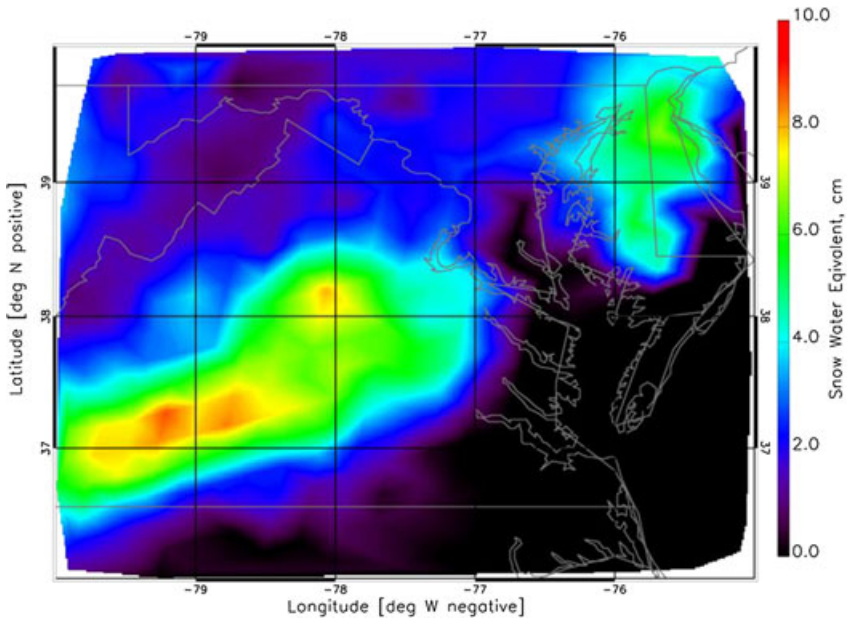

Figure 10. Special Sensor Microwave Imager/Sounder snow image for 12 February 2010

DOI: 10.1002/hyp

the month) and orbital swath gaps over the Baltimore/Washington area. Of course, it is less than ideal to evaluate large-scale remotely sensed data with point data (stations).

DISCUSSION

In general, the results of this particular case study show promise that falling snow detection and SWE derivations are possible in the rather complex physiographic conditions found in the Baltimore/Washington DC area. Increases in SD and SWE were retrieved following the extreme snowfall events detected in early February 2010. Nonetheless, interpretation of the passive microwave SWE results is complicated by the changing snowpack conditions and on the days of the biggest snows, by the intensity of the snowfall and/or the presence of liquid water within the storm clouds (Rosenkranz, *et al*., 1982). Because of the extreme heterogeneity of the surface and atmospheric features over much of the study area combined with the lack of ground truth, there is a degree of conjecture regarding the discussion of the results.

On the two days having extremely heavy snowfalls (snow falling in temperatures not far from 0 °C and at rates >2.5 cm/h), SWE from AMSR-E was not retrieved (Figures 7 and 8). SWE retrievals from the AMSR-E measurements (algorithm) on 6 February, near 0740 UTC, and on 10 February, near 0716 UTC, as presented above, apparently failed during the passage of these snowstorms. As an aside, Figures 5 and 6 show that there were difficulties detecting the full spatial extent of the 6 February heavy snow events because of a drier atmosphere at height in central and southern Virginia.

Figure 11(A) (6 February) and (B) (10 February) examines the SWE issues in more detail by showing the evolution of the snowfall events on the basis of the 89, 150 and 183.3 ± 7 GHz channels of MHS, Meteorological Operational Satellite Programs A and Special Sensor

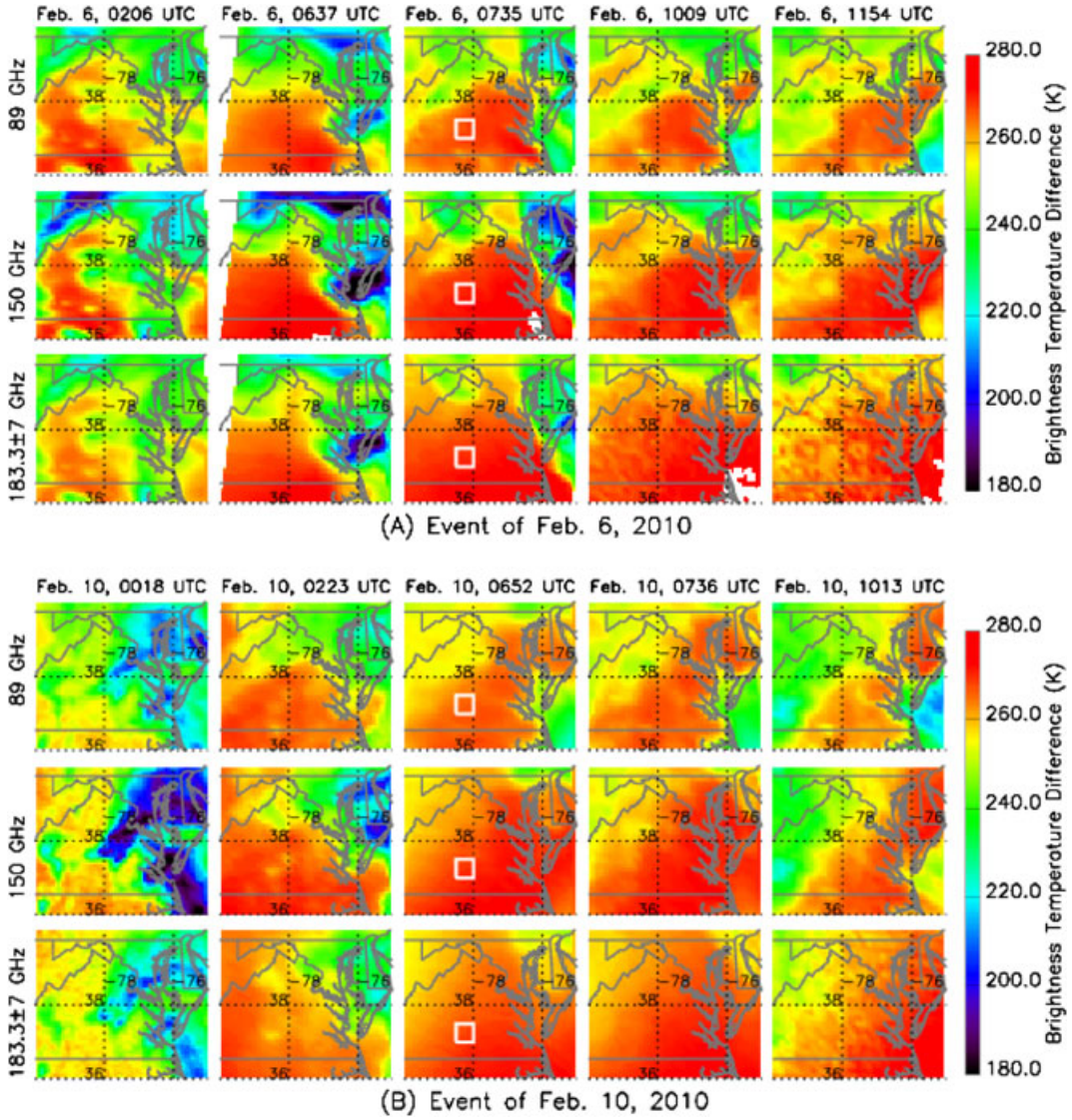

Figure 11. (A) and (B) for 6 and 10 February, respectively, showing the evolution of the snowfall events on the basis of the 89, 150 and 183.3 ± 7 GHz channels of Microwave Humidity Sounder, Meteorological Operational Polar Satellite-2 and Special Sensor Microwave Imager/Sounder of Advanced Microwave Sounding Unit-B. In the third column of both (A) and (B), a small area enclosed by the small white square in each map is selected for the calculations of average brightness temperature of several Microwave Scanning Radiometer and Advanced Microwave Sounding Unit-B/Microwave Humidity Sounder channels described in the text

DOI: 10.1002/hyp

Microwave Imager/Sounder sensors of AMSU-B. Five measurements (displayed as columns) from these high-frequency channels over the approximate 10-h period centred on the AMSR-E measurements have been selected for illustration. For each event, three rows from top to bottom give the Tb maps of the region in pseudocolour for the 89 (or 92H for the Special Sensor Microwave Imager/Sounder), 150 and 183.3 ± 7 GHz, respectively. Note that the 150 GHz channel clearly shows the strongest snowfall signals for both events – it has considerably less water vapour absorption compared with the 183.3 ± 7 GHz channel.

The first column of Figure 11 (A) shows that at 0206 UTC on 6 February, the snowfall event began to move out of central Virginia on the basis of these high-frequency channels and the images in Figures 4 and 5. By 0637 UTC, the snowfall signatures were mostly limited to northern Virginia, central Maryland and to the northern areas of the Delmarva Peninsula. The surface features for most of Virginia were not visible from all channels, apparently masked by the trailing cloud cover; the 89, 150 and 183.3 ± 7 GHz channels showed nearly identical Tbs. The Tb values averaged over a small area, as indicated by the squares in the third column of Figure 11(A) and selected in correspondence to high SWE retrievals on 7 and 8 February (Figure 7), give values of 268, 271 and 270 K at 89, 150 and 183.3 ± 7 GHz, respectively. The closeness in Tbs between the 150 and 183.3 ± 7 GHz channels strongly suggests absorption of radiation by low-level liquid clouds or by precipitation (Rosenkrantz *et al*., 1982). The corresponding AMSR-E measurements over the same area at 0740 UTC give 265, 259, 266, 262, 272 and 271 K at 18.7 V, 18.7 H, 36.5 V, 36.5 H, 89 V and 89 H GHz, respectively. The 36.5 GHz Tbs, for either vertical or horizontal polarization, are slightly higher than those at 18.7 GHz – no snow is detected.

The evolution of the 10 February event shown in Figure 11(B) is quite similar to that of the 6 February event. The Tb maps in the first column show that the snowfall began to move out of the region at 0018 UTC. By 0223 UTC, snowfall was already east of the Chesapeake Bay. Between 0652 UTC and 0736 UTC, the 89, 150 and 183.3 ± 7 GHz channels again showed nearly identical Tbs. The average Tbs over the same selected area as in (A) give 266, 269 and 268 K for the 89, 150 and 183.3 ± 7 GHz channels, respectively. The closeness of the Tbs among these channels again suggests low-level, liquid cloud absorption. The corresponding AMSR-E average Tbs near 0716 UTC over the same area are 264, 261, 266, 263, 271 and 270 K for the 18.7 V, 18.7 H, 36.5 V, 36.5 H, 89 V and 89 h GHz channels, respectively. For either polarization, the Tb values at 36.5 GHz are higher than those at 18.7 GHz.

For both events, the clouds containing liquid water apparently play a major role in the failure of the AMSR-E to retrieve SWE. The presence of liquid in the clouds also affects the performance of the falling snow detection because when liquid is present, events are screened out of the detection process. The absorption coefficient of liquid clouds is approximately proportional to the square of the frequency (Staelin *et al*., 1976), and because of this effect, it has been shown that the presence of such clouds strongly impacts the sensitivity of estimating SWE using the radiometric measurements near 19 and 37 GHz (Wang and Tedesco, 2007). This absorption-related increase in AMSR-E Tbs at 18 and 36.5 GHz exceeded the algorithm's designated SWE threshold detection values for these channels, thus rendering the retrieval ineffective.

Referring back to Figures 3 and 4 where the evolution of snowfalls from the first event based on ground observations at CHO, IAD and BWI were displayed, the northeastward movement of the storm could be clearly identified. At CHO, snowfall began before 5 February, peaked ~1600 h (0100 UTC on 6 February), well before the time of the first column displayed in Figure 11(A). By ~0500 UTC on 6 February, the intensity of the snowfall dropped down to ~ threshold of detection. As the storm moved northeastward and deepened, with intensity peaking ~0600 UTC, snow accumulations increased rapidly at BWI. The snowfall intensity reached a brief minimum at ~1300 UTC before rising again to a moderate level. Snow continued to fall in the Baltimore/Washington area for another 3–4 h before stopping. The pattern of snowfall at IAD was quite similar to the pattern at CHO and BWI, although the intensity was not as great. The intensity here was, in general, between that of CHO and BWI, indicating the storm's northeastward movement. All together, the snowfall at BWI lasted several hours longer than at CHO, and total accumulations were considerably higher at BWI (63 cm) than at CHO (32 cm). The time history of Figure 3 during 0200–1200 UTC on 6 February appeared to be relatively consistent with the progression of the snowfall pattern displayed in Figure 11(A) near these two stations – low Tbs in all three channels.

Following the two big snow events, retrieved SWE values in northern Virginia and central Maryland were suppressed in early to middle February when a deep snowpack was in place and buoyed later in the month and in early March when the pack was ablating (Figures 7 and 8). Differences in snow crystal characteristics might either suppress or boost retrieved SWE values, but it is unlikely that changes in crystal structure as the snowpack evolves are solely responsible for the somewhat perplexing results noted here. It should be mentioned that Radio Frequency Interference was investigated and is unlikely to play a role in the reduced retrieved SWE amounts observed in the densely populated Baltimore/Washington urban complex. Radio Frequency Interference has previously been observed to affect SWE and snowfall derivations (primarily at 10 GHz) in and nearby large cities (Kelly *et al*., 2003; Kidd, 2006). Another complication is directive effect of building structures in an urban environment that can change the overall emissivity of snow-covered urban areas.

In northern North Carolina and southern Virginia, sleet and freezing rain mixed in with falling snow during the two big storms, whereas further to the north, nearly all of the precipitation fell as snow. In southern areas, it is possible that retrieved SWE corresponds to the state of

DOI: 10.1002/hyp

the snowpack at the time precipitation was falling rather than to the actual depth of the snowpack and SWE. The glaze or glassy surface that ensued following the icy precipitation mix increased scattering, thus lowering Tb and boosting the retrieved SWE values (Hall *et al*., 1984).

Later in February, in northern Virginia, Maryland and southern Pennsylvania, snow that melted and then refroze formed a surface layer of more than a centimetre in thickness. Very little additional snowfall accumulated on this layer, which behaved similarly to the icy surface further to the south at middle month. Therefore, the retrieved SWE values here as well as in south central and southwestern Virginia were overestimated – the lower Tbs were not entirely because of increased SWE but rather to how the microwave signals were affected by icy surfaces. See also Grenfell and Putkonen (2008) and Rees *et al*. (2010).

The snowpack was melting from 21 to 24 February but was still in place later in the month despite the absence of a retrieved SWE signature on 23 and 24 February (Figures 7 and 8). Above-freezing maximum temperatures of between 6 and 8 °C and just above freezing minimum temperatures slightly melted the pack on these days, obscuring it from the AMSR-E sensor. When the air temperature is at or above 0 °C, the emissivity of a snowpack increases with a corresponding increase in Tb. Just 3% liquid water content will radically affect the imaginary part of the dielectric constant of snow, significantly increasing the snow absorption/emission, resulting in higher Tb values for the same mass of snow (Foster *et al*., 1997).

Falling snow observations and retrievals show that falling snow signatures can be detected in high frequency Tbs. It is encouraging that where falling snow is detected (6 February – Figures 4 and 5), higher snowpack SWEs are retrieved the next day. This study demonstrates that the improved snowfall detection algorithm performs well when there is sufficient water vapour in the atmosphere. For example, snow is detected in Figure 5 and is associated with limited ground truth (solid black stars depicted in Figure 5), with greater consistency when Figure 6 indicates a more moist atmosphere.

CONCLUSIONS

This study shows that despite the high variability of the area being observed, there is consistency between falling snow and snowpack retrievals. Where snowfall was detected, SD and SWE were retrieved. However, both the snowfall detection and SWE algorithms suffered because of the high variability of snowfall intensity and accumulation as well as the complex surface features in the Baltimore/Washington area. On the two days when intense snowfalls occurred, 6 and 10 February 2010, retrievals of SWE were compromised. This was likely a result of thermal emission from water droplets in low-level clouds within portions of the storm, which acted to increase AMSR-E Tbs, thereby rendering minimal or zero values for SWE. The presence of such clouds strongly impacts the sensitivity of estimating SWE using radiometric measurements near 19 and 37 GHz. Glaze or icy layers within and on the surface of the snowpack served to increase scattering, thus lowering Tb and boosting the retrieved SWE values, first in southern portions of the study area and then further north as the month of February progressed.

The performance of the SWE algorithm is uneven because of the complexity and variability of the snowpack and especially because it is likely that icy surfaces resulted in an overestimation of SWE. Although features including vegetation, terrain, open water and melting snow can confound microwave algorithms, signatures indicative of a substantial snowpack were observed following the historical February snowstorms. It should be mentioned that intense storms such as these are not necessarily the ideal events for a complete algorithm evaluation. Although the near optimal conditions permitted us to examine snowfall and SWE where falling snow and snow on the ground were well documented (if not well instrumented), reliable remote sensing techniques must capture nominal as well as extreme snow events.

Falling snow observations and retrievals show that, indeed, falling snow signatures can be observed in high frequency Tbs. The performance of the falling snow detection was shown to be dependent on a few factors including snow intensity and environmental conditions. Light falling snow cannot be detected because the signal is weak and environmental conditions such as dry air mass incursions in the middle troposphere inhibit the detection of falling snow. Performance of this algorithm is expected to improve with additional knowledge about falling snow intensity and the environmental conditions. Research is ongoing to develop new approaches for detecting snowfall in drier atmospheric conditions and to handle the widely varying precipitation signatures. With five operational satellites and up to ten global observations each day, the AMSU/MHS snowfall product provides valuable and first-of-its-kind information on winter precipitation at timescales of interest for this study.

It is expected that both the falling snow and snowpack algorithms would be improved by combining the separate retrievals. Making the algorithms more complementary and physically based should be one of the main thrusts of future efforts in this research area. Planning a field campaign to look more closely at both falling snow characteristics and snowpack properties is an important part of continuing this work. The February 2010 case study investigated here can be used as a starting point to pursue this further. Studies such as this will be valuable in the build-up to NASA's Global Precipitation Mission and, if chosen, to the next European Space Agency Earth Explorer, the CoREH20 Mission.

ACKNOWLEDGEMENTS

The authors are most appreciative of the referees' efforts in helping to make this a stronger paper. We are also grateful to Dr Richard Kelly (University of Waterloo, Waterloo, Ontario, Canada) for his helpful comments. Research carried out at JPL and GSFC was supported by the

DOI: 10.1002/hyp

NASA Terrestrial Hydrology and also the Precipitation Measurement Missions Programs. Quality Controlled Local Climatological Data snow accumulation observations are from NOAA/National Climatic Data Center (NCDC) and AMSU-B/MHS data from the CLASS data system. Judah Cohen is supported by the National Science Foundation grants ARC-0909459 and ARC-0909457. Research carried out at the Jet Propulsion Laboratory, California Institute of Technology and at the Goddard Space Flight Center was supported by the NASA Terrestrial Hydrology and also the Precipitation Measurement Missions Programs.

REFERENCES

Baldwin MP, Dunkerton TJ. 1999. Propagation of the Arctic Oscillation from the stratosphere to the troposphere. *Journal of Geophysical Research* **104**: 30937–309346.

Baldwin MP, Dunkerton TJ. 2001. Stratospheric harbingers of anomalous weather regimes. *Science* **294**: 581–584.

Brown R, Braaten R. 1998. Spatial and temporal variability of Canadian monthly snow depths, 1946–1995. *Atmosphere-Ocean* **36**(1): 37–45.

Chang ATC, Kelly REJ, Josberger EG, Armstrong RL, Foster JL, Hall DK. 2005. Analysis of gauge-measured and passive microwave derived snow depth variations of snowfields. *Journal of Hydrometeorology* **6**: 20–33.

Chen FW, Staelin DH. 2003. AIRS/AMSU/HSB precipitation estimates. *IEEE Transactions on Geoscience and Remote Sensing* **41**: 410–417.

Clifford D. 2010. Global estimates of snow water equivalent from passive microwave instruments: history, challenges and future developments. *International Journal of Remote Sensing* **31**(14): 3707—3726.

Cohen J, Foster J, Barlow M, Saito K, Jones J. 2010. Winter 2009/10: a case study of an extreme Arctic Oscillation event. *Geophysical Research Letters* **37**: L17707, doi: 10.1029/2010GL044256.

Davenport IJ, Sandells MJ, Gurney RJ. 2010. The effects of variation in snow properties on snow mass estimation using the Chang algorithm. In *Proceedings of the Third International Symposium of the British Hydrological Society, 19–23 July 2010*, Newcastle, UK.

Derksen C, LeDrew E, Goodison B. 2000. Temporal and spatial variability of North American Prairie snow cover (1988 to 1995) inferred from passive microwave derived snow water equivalent (SWE) imagery, *Water Resources Research* **36**(1): 255–266.

Ferraro RR, Weng F, Grody NC, Zhao L, Meng H, Kongoli C, Pellegrino P, Qiu S, Dean C. 2005. NOAA operational hydrological products derived from the advanced microwave sounding unit. *IEEE Transactions on Geoscience and Remote Sensing* **43**: 1036–1049.

Foster JL. 1995. Improving and evaluatiung remotely-sensed snow/microwave algorithms and snow output from general circulation models, Ph.D Dissertation (Chapter 2), University of Reading.

Foster JL, Chang ATC, Hall DK. 1997. Comparison of snow mass estimates from a prototype passive microwave snow algorithm, a revised algorithm and a snow depth climatology. *Remote Sensing of Environment* **62**: 132–142.

Foster JL, Hall DK, Chang ATC, Rango A. 1984. An overview of passive microwave snow research and results. *Reviews of Geophysics and Space Physics* **22**(2): 195–208, 1984.

Foster J, Sun C, Walker J, Kelly R, Chang A, Dong J, Powell H. 2005. Quantifying the uncertainty in passive microwave snow water equivalent observations. *Remote Sensing of Environment* **94**: 187–203.

Grenfell T, Putkonen J. 2008. A method for the detection of the severe rain-on-snow event on Banks Island, October 2003, using passive microwave remote sensing. *Water Resources Research* **44**: W03425, doi: 10.1029/2007SR005929.

Gutowski WJ, Hegerl GC, Holland GJ, Knutson TR, Mearns LO, Stouffer RJ, Webster PJ, Wehner MF, Zwiers FW. 2008. Causes of observed changes in extremes and projections of future changes. In: *Weather and Climate Extremes in a Changing Climate: Regions of Focus: North America, Hawaii, Caribbean, and U.S. Pacific Islands*, Karl TR, Meehl GA, Miller CD, Hassol SJ, Waple AM, Murray WL (eds). Synthesis and Assessment Product 3.3. U.S. Climate Change Science Program, Washington, DC; 81–116.

Hall DK, Foster JL, Chang ATC. 1984. Nimbus-7 SMMR polarization responses to snow depth in the mid western U.S . *Nordic Hydrology* **15**: 1–8.

Hallikainen M, Halme P, Lahtinen P, Pulliainen J. 2004. Retrieval of snow characteristics from spaceborne scatterometer data, In *Proc. of IEEE Geoscience and Remote Sensing Symposium*, IGARSS 2004, Anchorage, Alaska, USA, Conference CD.

Hansen MC, DeFries RS, Townshend JRG, Carroll M, Dimiceli C, Sohlberg RA. 2003. Global percent tree cover at a spatial resolution of 500 meters: first results of the MODIS vegetation continuous fields algorithm. *Earth Interactions* **7**(10): 1–15.

Kelly REJ. 2009. The AMSR-E snow depth algorithm: description and initial results. *Journal of the Remote Sensing Society of Japan* **29**(1): 307–317.

Kelly REJ, Chang ATC, Tsang L, Foster JL. 2003. A prototype AMSR-E global snow area and snow depth algorithm. *IEEE Transactions on Geoscience and Remote Sensing*, EO-1 Special Issue, **41**(2): 230–242.

Kidd C. 2006. Radio frequency interference at passive microwave earth observation frequencies. *International Journal of Remote Sensing* **27** (18): 3853–3865.

Kocin P, Uccellini L. 2004a. Northeast snowstorms. *American Meteorological Society* ISBN 1878220640.

Kocin PJ, Uccellini LW. 2004b. A snowfall impact scale derived from northeast storm snowfall distributions. *Bulletin of the American Meteorological Society* DOI: 10.1175/BAMS-85-2-177; An online supplement to this article can be found at DOI: 10.1175/BAMS-85-2-kocin.

Kongoli C, Pellegrino P, Ferraro RR, Grody NC, Meng H. 2003. A new snowfall detection algorithm over land using measurements from the Advanced Microwave Sounding Unit (AMSU). *Geophysical Research Letters* **30**(14): 1756, doi: 10.1029/2003GL017177.

NOAA, February. 2010. Temperature, precipitation and snowfall data for DCA, BWI, IAD, Charlottesville and Martinsburg.

Noh Y-J, Liu G, Jones AS, Vonder Haar TH. 2009. Toward snowfall retrieval over land by combining satellite and in situ measurements. *Journal of Geophysical Research* **114**: D24205, doi: 10.1029/2009JD012307.

Rees A, Lemmetyinen J, Derksen C, Pulliainen J, English M. 2010. Observed and modelled effects of ice lens formation on passive microwave brightness temperatures over snow covered tundra. *Remote Sensing of Environment* **114**: 116–126.

Rosenkranz PW, Komichak MJ, Staelin DH. 1982. A method for estimation of atmospheric water vapor profiles by microwave radiometry . *J. Appl. Met.* **21**: 1364–1370.

Seager R, Kushnir Y, Nakamura J, Ting M, Naik N. 2010. Northern Hemisphere winter snow anomalies: ENSO, NAO and the winter of 2009/10. *Geophysical Research Letters* **37**: L14703, doi: 10.1029/2010GL043830.

Skofronick-Jackson G, Benjamin TJ. 2011. Surface and atmospheric contributions to passive microwave brightness temperatures for falling snow events. *J. Geophys. Res.* **116**: D02213, doi: 10.1029/2010JD014438.

Skofronick-Jackson G, Kim M-J,Weinman JA, Chang DE. 2004. A physical model to determine snowfall over land by microwave radiometry, *IEEE Transactions on Geoscience and Remote Sensing* **42**: 1047–1058.

Smith BG (ed). 2010. Washington-Baltimore climate review, February 2010. http://www.weather.gov/os/presto/presto2010/2010feb.pdf

Staelin DH, Kunzi KF, Pettyjohn RL, Poon RKL, Wilcox RW. 1976. Remote sensing of atmospheric water vapor and liquid water with the Nimbus 5 microwave radiometer. *Journal of Applied Meteorology* **15**: 1204–1214.

Sturm M, Holmgren J, Liston GE. 1995. A seasonal snow cover classification system for local to regional applications. *Journal of Climate* **8**: 1261–1283.

Tedesco M, Reichle R, Low A, Markus T, Foster JL. 2010. Dynamic approaches for snow depth retrieval from space-borne microwave brightness temperature. *IEEE Transactions on Geoscience and Remote Sensing* **48**: 1955–1967.

Thompson DWJ, Wallace JM. 2000. Annular modes in the extratropical circulation. Part I: month-to-month variability. *Journal of Climate* **13**: 1000–1016.

Uccellini L, Petersen R, Brill K, Kocin P, Tuccillo J. 1987. Synergistic interactions between an upper level jet streak and diabatic processes that influence the development of a low-level jet and a secondary coastal cyclone. *Monthly Weather Review* **115**: 2227–2261.

Walker AE, Goodison B. 2000. Challenges in determining snow water equivalent over Canada using microwave radiometry, Proceedings of IGARSS 2000, Honolulu, HI, 24–28 July 2000.

Wang JR, Tedesco M. 2007. Identification of atmospheric influences on the estimation of snow water equivalent from AMSR-E measurements. *Remote Sensing of Environment* **111**: 398–408.

Yan B, Weng F, Meng H. 2008. Retrieval of snow surface microwave emissivity from the advanced microwave sounding unit *Journal of Geophysical Research* **113**: D19206, doi: 10.1029/2007JD009559